OPEN ACCESS

# Low-field magnetovoltage measurements in superconducting $Y_1Ba_2Cu_3O_{7-\delta}$

New Journal of Physics
The open-access journal for physics

# Low-field magnetovoltage measurements in superconducting $Y_1Ba_2Cu_3O_{7-\delta}$

**A Kiliç**[1], **K Kiliç, H Yetiş and O Çetin**
Department of Physics, Turgut Gulez Research Laboratory, Abant Izzet Baysal University, 14280 Bolu, Turkey
E-mail: kilic_a@ibu.edu.tr

*New Journal of Physics* **7** (2005) 212
Received 5 July 2005
Published 7 October 2005
Online at http://www.njp.org/
doi:10.1088/1367-2630/7/1/212

**Abstract.** We investigated the influences of field orientation with respect to transport current, magnitude of transport current, temperature and field-sweep rate ($dH/dt$) on the evolution of magnetovoltage ($V$–$H$) curves in polycrystalline superconducting bulk sample of $Y_1Ba_2Cu_3O_{7-\delta}$. In well-defined magnetic field and temperature ranges, it was found that a relative decrease in dissipation could be obtained depending on the current as the field-sweep rate decreases, so that it underlines the importance of time spent to plot the whole cycle of $V$–$H$ curves. This physical observation was correlated to more effective field and less relaxation evolving in the grains and more return flux and less effective field at the grain boundaries. On the other hand, an enhancement in hysteresis effects in $V$–$H$ curves which manifests itself as an increase in the area enclosed by the hysteresis loop was observed at low currents and at low temperatures. These behaviours were attributed to the increase in effective trapped field originated from the relative increase in the height of pinning barriers due to the low currents, and low-thermal fluctuations together with flux creep appearing at low temperatures. Finally, the strong clockwise hysteresis effects in $V$–$H$ curves were interpreted within the granularity of sample mainly in terms of flux trapped in the grains returning through the grain boundaries.

[1] Author to whom any correspondence should be addressed.


PII: S1367-2630(05)03161-7

## Contents



## 1. Introduction

It is well known that the flux dynamics in polycrystalline high-$T_C$ ceramic superconductors (HTSCs) is rather complicated and unusual. Therefore, significant efforts have been devoted to the investigation of their transport and magnetic properties [1]–[38]. One of the main properties of polycrystalline HTSCs is that the dissipation is, in general, dominated by weakly linked grain boundaries and partly by the grains [1, 2], [4]–[6], [10, 11], [16]–[18], [22]–[24], [36]. Both experimental [1, 2], [4]–[6], [10, 11], [16]–[18], [22, 36] and theoretical studies [5, 17, 33, 36, 37] reveal that the structural disorder and intrinsic character of grain boundaries have a direct effect on the current carrying capacity of HTSCs. In these regions, the local superconducting order parameter is strongly suppressed due to the chemical and anisotropic properties of grains and their boundaries [16, 17, 36]. In addition, the physical situation developing in these regions depends on the misorientation angle between the adjacent grains [11, 36]. These are the main reasons why the strong-field dependence of the intergranular currents were observed in polycrystalline HTSC samples.

It is still challenging to improve the structural properties of the grain boundaries, and there is a requirement to get information about the properties of grain boundaries for the possible practical applications of HTSCs. Therefore, to understand the basic structural properties of interfaces, bicrystal technology which allows to fabricate well-defined grain boundaries, bi-epitaxial growth, step-edge technology have been developed [11, 36, 38].

On the other hand, for large-scale applications of HTSCs, recent advances which are very promising are focused on the improvement of long-coated superconducting wires with high critical current densities [39, 40]. In the fabrication of long wires, one of the main problems

is the influence of grain boundaries obstructing the current flow. Therefore, performance of coated HTSCs is limited to the improvement of grain boundaries and the presence of low-angle grain boundaries [40, 41]. The transport measurements and, in particular, magneto-optical imaging studies reveal that the flux lines percolate through low-grain boundaries of the polycrystalline network and encounter many obstructions exhibiting a complex pattern together with inhomogeneous distribution along the sample [40], [42]–[45]. For practical applications, Larbalastier *et al* [40] discussed to enhance the current carrying capacity of the superconducting materials, i.e., $Y_1Ba_2Cu_3O_{7-\delta}$ (YBCO) and $(Bi,Pb)_2Sr_2Ca_2Cu_3O_x$ so that the grain–grain misalignment must be held to values of 5° or less. Norton *et al* [41] fabricated high-quality YBCO films on biaxially textured nickel (Ni) (0 0 1) substrates of re-crystallized and cold rolled Ni by using pulsed laser deposition. The obtained results are comparable to that of epitaxially grown thin films of YBCO on single-crystalline oxide substrates and very promising for high-field applications at liquid nitrogen temperatures.

The transport and magnetization measurements in HTSCs [1, 2, 17], [22]–[24], [46]–[59] and low-temperature superconductors (LTSCs) [60]–[63] exhibit strong irreversibilities depending on the temperature and external magnetic-field ranges to be investigated. The irreversibility in polycrystalline HTSC samples manifests itself not only in magnetization measurements [1, 17], [46]–[51], but also in magnetoresistance [52]–[58], transport critical current density [52, 57], current–voltage ($I$–$V$) curves [59] at low-, moderate- and high-field ranges. The hysteretic effects in magnetoresistance measurements appear in the clockwise direction as the external field is swept up and down [22], [53]–[58]. Generally, low- and high-field strong irreversibilities seen in polycrystalline HTSC samples are interpreted in terms of flux trapping, developing both intergranular and intragranular regions [22], [53]–[58]. Ji *et al* [22] proposed an analytical model, the so-called two-level critical state model, by calculating the macroscopic and local fields for ordered and disordered polycrystalline samples. In this model, it has been assumed that the flux dynamics is maintained by the percolative paths through the grains. The model gives reasonable agreements with the microwave losses in granular materials and also explains the magnetic hysteresis effects. Furthermore, a recent model for high-field magnetoresistance of granular samples has been developed by Beloborodov *et al* [64] so that the model gives a reasonable agreement with the experimental results concerning the negative magnetoresistance observed in granular superconducting Al sample [65]. Recently, Palau *et al* [42] showed that the irreversibility effects arise from the return field from grains into the grain boundaries.

For practical applications of HTSCs, determination of the irreversibility line and its consequences are of great importance. The irreversibility line is defined as a borderline between the reversible (i.e., $J_c = 0$) and irreversible ($J_c \neq 0$) regions in the temperature versus magnetic-field plane, where $J_c$ is the critical current density [17]. In this plane, the irreversibility line separates the flux solid phase with vortices pinned and the flux liquid phase where many vortices are unpinned or free to move with dissipation. The irreversibility line represent a crossover region from flux creep to thermally assisted flux flow and to flux flow, and may be affected by sample-dependent properties such as the nature and density of pinning centres, intrinsic and extrinsic anisotropy. Its investigation is of importance for understanding of flux-line lattice behaviour and irreversibilities caused by different mechanisms. It is also crucial for the practical applications of the superconductors. For this purpose, it is needed to shift the irreversibility line to higher temperatures by improving the pinning properties of material, which leads to an enhancement in the current carrying capacity of the material [66].

In order to determine the vortex-phase transitions and dimensionality, nonlocal transport phenomena in a mixed state of a type-II superconductor, one of the powerful methods is the dc flux transformer technique based on the multiterminal contact configuration [67]–[71]. Lopez *et al* [68] carried out transport measurements in the mixed state of single-crystalline sample of YBCO by using dc flux transformer technique and showed that the vortex-phase transition is three-dimensional at the irreversibility line. A similar study on the same sample was performed by Grigera *et al* [70]. These researchers provided an evidence of a transition from liquid to smectic phase when the flux lines are subject to an attractive pinning potential.

The detailed transport measurements reveal that the motion of flux lines at low- and moderate-dissipation levels develops in the form of defective flow patterns, i.e., plastic motion, whereas, at high-dissipation levels, the motion becomes correlated and gives a unique vortex velocity [26, 62], [72]–[75]. As a result of the plastic flow of the flux lines, the moving state becomes sometimes noisy and also history dependent [75, 76]. In addition, the recent experimental studies show that there is a dynamic process in transport measurements, which causes peculiar time effects [59], [73]–[75], [77]. Kiliç *et al* [59, 74, 75, 77] showed that the dynamic effects in transport measurements carried out in polycrystalline bulk YBCO samples could be monitored experimentally by the time evolution of the sample voltage. Such time effects in transport measurements could be observed experimentally in $I$–$V$ curves of polycrystalline [68] and single-crystalline HTSC samples [25, 26] by several researchers. We note that the transport relaxation effects have also been observed for LTSC samples [73, 79]. For instance, Xiao *et al* [73] reported that there is a ramping-rate dependence in the $I$–$V$ curves of a field cooled single-crystalline 2H-$NbSe_2$sample. Such a ramping-rate dependence gives significant time effects. The experimental studies show that the speed of measurement in taking the data becomes an important parameter in transport measurements as in the case of the magnetization measurements ($M$–$H$), too [17, 59, 73]. The effect of current ramping rate and the flux creep on the transport properties of type-II superconductors have been investigated by Zhang *et al* [80] by solving numerically the nonlinear diffusion equation in one-dimension. The numerical results obtained by them and their experimental observations support that there is a remarkable time effects in transport measurements. We note that flux creep phenomenon is one of the most prominent features of HTSCs and reflects itself as high-relaxation rates in irreversible magnetization ($M_{\mathrm{irr}}$–$t$) and also in transport measurements so that it limits their potential applications. The modified versions of conventional flux creep theory, such as the collective creep theory developed by Feigel'man *et al* [81], give a general description which characterizes the $M_{\mathrm{irr}}$–$t$ dependence. In addition, in order to explain the unusual time effects in transport measurements, a new model called the two kinds of flux creep model has been proposed by Ma *et al* [82]. Flux creep occurs due to a finite resistivity, where the applied current is less than the critical one, and the flux motion is characterized by thermally activated hopping of uncorrelated flux lines (or bundles) over the pinning barriers. Due to the random distribution of pinning centres, such a flux motion can be directional and diffusive in character under the action of the Lorentz force. Thus, it results in spatially inhomogeneous flux distribution through the sample and can cause the formation of several dynamical phases of the vortices which are related to the plastic flow, immobile or pinned flux-line configuration [17, 80].

In this paper, we present magnetovoltage measurements ($V$–$H$ curves) carried out as a function of parallel and perpendicular magnetic-field ($H$) orientations with respect to the

transport current ($I$) (i.e., $\vec{H} \parallel \vec{I}$ and $\vec{H} \perp \vec{I}$), temperature, the magnitude of transport current, and sweep rate ($\mathrm{d}H/\mathrm{d}t$) of the external magnetic field in polycrystalline bulk sample of YBCO. The measurements reveal that the low-temperature ranges and low currents enhance the hysteresis effects in $V$–$H$ curves, which implies that, within the granularity of sample, the flux trapping is the main reason of irreversibilities appearing in $V$–$H$ curves. This paper also demonstrates that, in well-defined magnetic field and temperature ranges, the observation of the time effects in $V$–$H$ curves becomes possible for different magnetic-field-sweep rates.

## 2. Experimental procedure

The polycrystalline bulk YBCO samples used in this study were prepared from high-purity powders of $Y_2O_3$, $BaCO_3$ and CuO by conventional solid-state reaction with a similar route as described in [59, 74, 75, 77]. The slab shaped for transport measurements had typical dimensions of length 4 mm, width 0.1 mm and thickness 0.2 mm. dc transport measurements were carried out using the four-probe method in a closed-cycle refrigerator (Oxford Instruments (OI), CCC1104), and the temperature were measured by a calibrated Rh–Fe 27 Ω thermometer (the calibration number is 31202). A temperature stability better than 10 mK was maintained during the measurements (ITC-503 temperature controller, OI). The sample voltage were measured by using a sensitive digital voltmeter (Keithley-182) with a resolution 1 nV, and a programmable current source (Keithley-220) were used in applying current. The voltmeter is triggered for a maximum resolution of 61/2 digits and its buffer is read directly within the integration time of 100 ms. The time spent at a measurement point is adjusted with respect to the integration time of the device and kept to be constant during the course of experiments. The speed of measurement is always greater than that of the field-sweep rate, otherwise, it is impossible to measure the sample voltage properly as the sweep rate of magnetic field is varied. Thus, the effect of such a relative change can be seen in magnetovoltage measurements. The magnetic field was generated by an electromagnet (OI, N100 electromagnet). In magnetovoltage measurements, the external magnetic field was orientated parallel ($\vec{H} \parallel \vec{I}$) and perpendicular ($\vec{H} \perp \vec{I}$) to the transport current. The YBCO sample whose results are presented in this paper has zero resistance at ∼92 K with a transition $\Delta T_c$ of about 3 K at zero applied field.

## 3. Experimental results

### *3.1. Evolution of $V$–$H$ curves at different magnetic-field orientations with respect to transport current ($\vec{H} \parallel \vec{I}$ and $\vec{H} \perp \vec{I}$)*

Figures 1(a)–(d) show the clockwise hysteretic magnetovoltage ($V$–$H$) measurements taken for the field-sweep rates of $\mathrm{d}H/\mathrm{d}t = 13$ and $1\ \mathrm{mT\,s^{-1}}$ at $T = 87$ K in polycrystalline bulk YBCO sample. The external magnetic field was orientated parallel to the transport current ($\vec{H} \parallel \vec{I}$) in figures 1(a) and (c), whereas, in figures 1(b) and (d), the field was perpendicular to the current ($\vec{H} \perp \vec{I}$). The longitudinal magnetovoltage $V_\parallel$ and transverse magnetovoltage $V_\perp$ curves for $\vec{H} \parallel \vec{I}$ and $\vec{H} \perp \vec{I}$, respectively, were obtained for the constant dc current values of $I = 10, 20$ and 30 mA by sweeping the external magnetic field up and down in a field range of 0–70 mT. In the figures, the arrows show the direction of sweeping of the magnetic field.

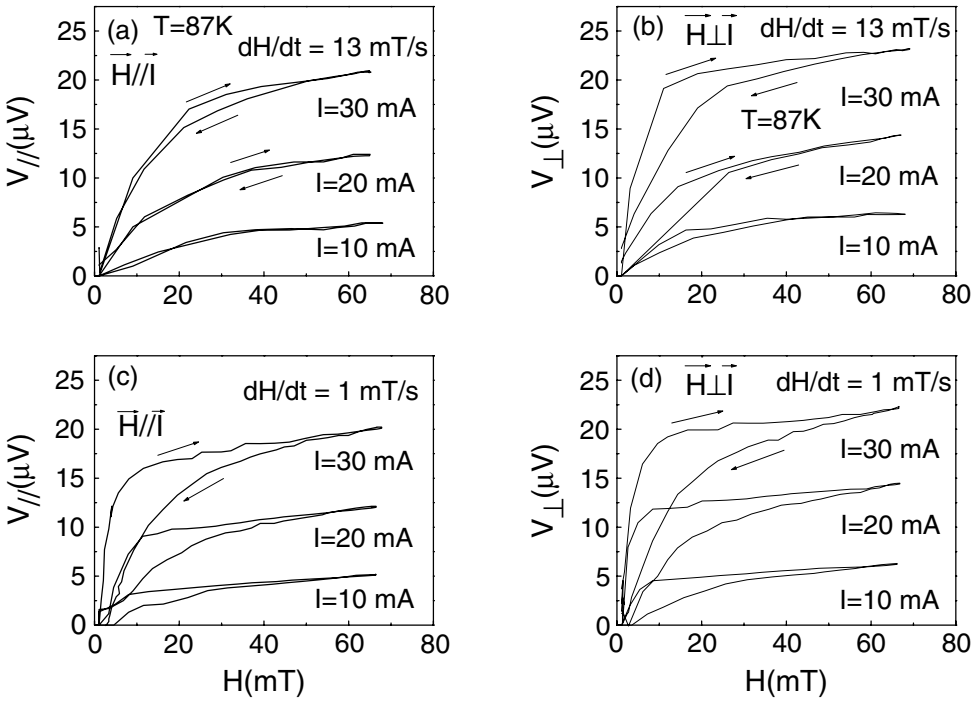


**Figure 1.** (a)–(d) Evolution of $V$–$H$ curves measured for $I = 10$, 20 and 30 mA at 87 K for the sweep rates of $\mathrm{d}H/\mathrm{d}t = 1$ and 13 mT s$^{-1}$. The field was orientated parallel ((a) and (c), $V_{\parallel}$ curves) and perpendicular ((b) and (d), $V_{\perp}$ curves) to the transport current. The arrows show the direction of the sweeping of the magnetic field.

The voltage corresponding to the longitudinal $V_{\parallel}$ and transverse $V_{\perp}$ magnetovoltage curves illustrated in figures 1(a)–(d) increases nonlinearly with increasing external magnetic field and tend to become nearly saturated. In figure 1(a), the $V_{\parallel}$ curves measured for $\mathrm{d}H/\mathrm{d}t = 13$ mT s$^{-1}$ exhibit nearly a reversible behaviour for the current values of 10 and 20 mA, whereas, for 30 mA, the hysteresis effect which manifests itself as a relative increase in the area enclosed by the curve appear weak. On the other hand, for the same sweep rate, the hysteresis effects become more significant in $V_{\perp}$ curves, in particular, for the current of 30 mA. It is seen that, in figure 1(b), the $V_{\perp}$ curves measured at $I = 10$ and 20 mA are nearly irreversible for the field values $H \lesssim 40$ mT and the irreversible behaviour extends to higher magnetic field ($H \sim 60$ mT) for $I = 30$ mA. Furthermore, figures 1(c) and (d) show that the hysteresis effects in the $V_{\parallel}$ and $V_{\perp}$ curves become more observable as the field-sweep rate of external field is decreased from 13 to 1 mT s$^{-1}$. These observations can be evaluated as an indication of that the hysteresis effects depend on the direction of the current relative to the magnetic field, the magnitude of applied current and the field-sweep rate.

It is also seen from the figures 1(a)–(d) that the dissipation grows up rapidly and nonlinearly after a critical-field value $H_{\mathrm{c}}^{\mathrm{up}}$, ($H_{\mathrm{c}}^{\mathrm{up}} \sim 2$ mT). The increase in voltage at the beginning slows down by tending relatively to saturate within the full-field scale while the field is increased above $H_{\mathrm{c}}^{\mathrm{up}}$. The rate of dissipation for the same current values in $V_{\parallel}$ curves becomes relatively small as compared to that of $V_{\perp}$ curves, and the tending to saturation shifts to higher field values. Another

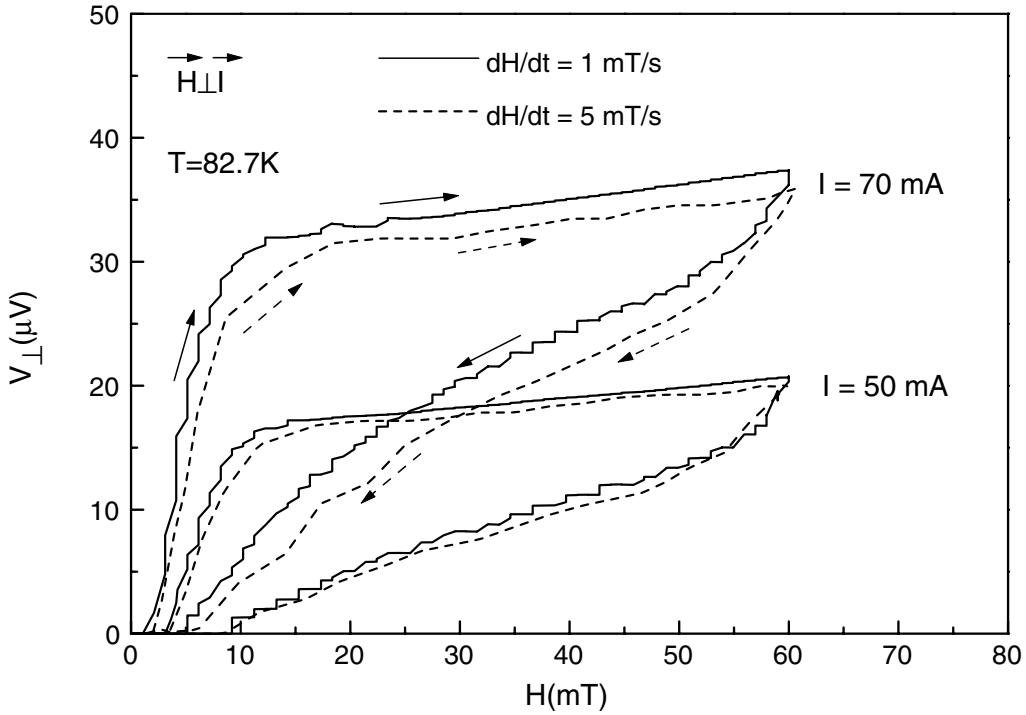


**Figure 2.** Sweep-rate dependence of the $V$–$H$ curves for $I = 50$ and 70 mA at 82.7 K. The solid lines represent the $V_\perp$–$H$ curves measured for $\mathrm{d}H/\mathrm{d}t = 1\,\mathrm{mT\,s^{-1}}$ and the dashed lines refer to the $V_\perp$–$H$ curves measured for $\mathrm{d}H/\mathrm{d}t = 5\,\mathrm{mT\,s^{-1}}$. The arrows show the direction of the sweeping of the magnetic field.

interesting behaviour seen in $V_\parallel$ curves is that there is a considerable dissipation which is nearly equal to $V_\perp$ curves, although the transport current and external magnetic field are parallel to each other.

### *3.2. Influence of temperature on the evolution of V–H curves at different field-sweep rates*

Figure 2 shows the influence of the sweeping rate of external magnetic field on the evolution of $V_\perp$–$H$ curves at 82.7 K. The measurements were performed at the currents $I = 70$ and 50 mA for $\mathrm{d}H/\mathrm{d}t = 1$ and $5\,\mathrm{mT\,s^{-1}}$, respectively. Note that the dissipation decreases with increasing $\mathrm{d}H/\mathrm{d}t$. In addition, the steps and plateaux for $\mathrm{d}H/\mathrm{d}t = 1\,\mathrm{mT\,s^{-1}}$ are more prominent as compared to that observed for $\mathrm{d}H/\mathrm{d}t = 5\,\mathrm{mT\,s^{-1}}$. A considerable decrease in the number of the steps and plateaux for $\mathrm{d}H/\mathrm{d}t = 5\,\mathrm{mT\,s^{-1}}$ develops, and, thus, the $V_\perp$ curves become more smooth. As is seen from the curves, $H_c{}^{up}$ increases slightly with increasing $\mathrm{d}H/\mathrm{d}t$ and this behaviour is more prominent in the curves measured for different values of $\mathrm{d}H/\mathrm{d}t$ at the constant larger values of the transport current. On the other hand, the $V_\perp$ curves measured for $I = 50$ and 70 mA represent a similar behaviour and the area of the hysteresis loops at each current value is nearly the same for both sweep rates, and, to increase the sweep rate by a factor of 5 does not cause any remarkable change in shape of the hysteresis loops, but results in a pronounced difference in measured dissipation of $V_\perp$–$H$ curves.

Figure 3 shows the temperature dependence of $V_\perp$–$H$ curves taken at the current values of $I = 30$ and 70 mA for 83 and 86 K. For all $V_\perp$ curves represented in this figure, the magnetic

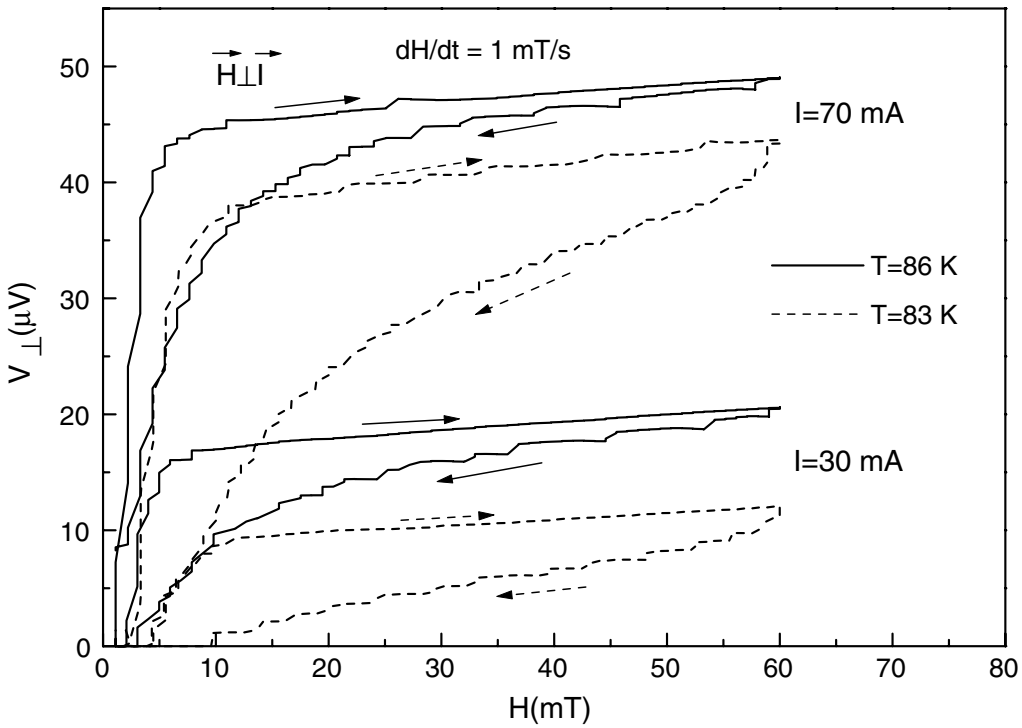


**Figure 3.** Influence of temperature on the evolution of the $V_{\perp}$–$H$ curves at $I = 30$ and 70 mA for the sweep rate $\mathrm{d}H/\mathrm{d}t = 1\,\mathrm{mT\,s^{-1}}$. The solid lines correspond to the $V_{\perp}$–$H$ curves measured at $T = 86\,\mathrm{K}$, whereas, the dashed lines represent the $V_{\perp}$–$H$ curves measured at $T = 83\,\mathrm{K}$. The arrows show the direction of the sweeping of the magnetic field.

field was swept up and down with a sweep rate of $\mathrm{d}H/\mathrm{d}t = 1\,\mathrm{mT\,s^{-1}}$. A direct comparison between the curves taken for the same current values reveals that the dissipation decreases and the irreversible behaviour becomes more pronounced as the temperature is reduced so that a considerable increase in the area of the hysteresis loops is observed as the temperature is varied from 86 to 83 K. As is noted, in the $V_{\perp}$ curves, the large plateaux are followed by small steps in the increasing branch of the hyteresis, whereas, the smaller plateaux with small steps are observed for decreasing branch. In addition, we note that the critical value of $H_{\mathrm{c}}^{\mathrm{up}}$ increases with a decrease in the temperature and current, separately.

### *3.3. Evolution of V–H curves upon sweeping of magnetic field in forward and reverse directions at different current values*

The temperature was decreased to 82 K and, this time, differently from the $V_{\perp}$–$H$ curves presented above, in the measurements, the magnetic field was swept in forward and reverse directions with a sweep rate of magnetic field, $\mathrm{d}H/\mathrm{d}t = 1\,\mathrm{mT\,s^{-1}}$, at each current value. Figure 4 shows a typical set of $V_{\perp}$ curves measured at different current values of $I = 30$, 40, 50, 60, 70 and 75 mA, respectively. The curves exhibit several different features as a function of transport current: it is seen that the $V_{\perp}$–$H$ curves evolve in the shape of a butterfly due to the variation in the direction of the external magnetic field. Strong irreversibilities appear together with a decrease in the

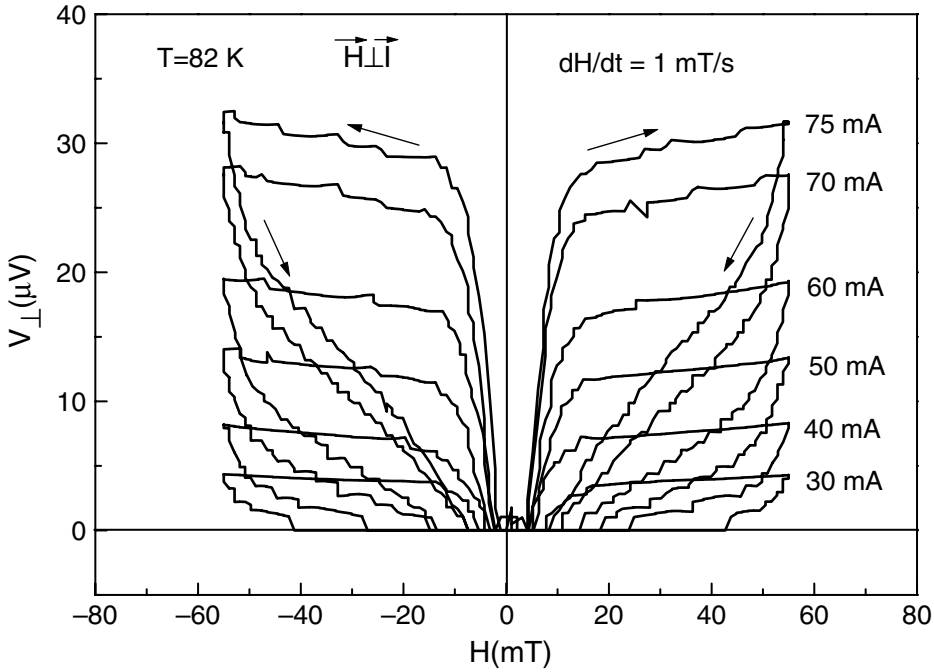


**Figure 4.** A set of hysteresis $V_{\perp}$–$H$ curves measured at different current values of $I = 30, 40, 50, 60, 70$ and 75 mA at $T = 82$ K for $\mathrm{d}H/\mathrm{d}t = 1\ \mathrm{mT\ s^{-1}}$. For each $V_{\perp}$–$H$ curves, the magnetic field is swept in forward and reverse directions under the constant transport current, respectively. The arrows show the direction of the sweeping of the magnetic field.

temperature with respect to other measurements depicted above. In the case of increasing field for both forward and reverse directions, the resistive state becomes observable after a certain critical value of the external magnetic field, $H_c^{up}$, and the dissipation sharply increases and tends to saturate, whereas, in the case of decreasing field in both forward and reverse directions, the sample becomes less resistive, and it recovers the zero resistance state at another critical value of the external magnetic field ($H_c^{down}$) which is greater than $H_c^{up}$. The experimental $V_{\perp}$–$H$ data reveal that $H_c^{up}$ and $H_c^{down}$ depend on the magnitude of the applied current. Figure 5 depicts such a dependence extracted from the sweeping of the magnetic field in forward direction. It is seen from figure 5 that both $H_c^{up}$ and $H_c^{down}$ decrease with increasing transport current. We suggest that the difference between $H_c^{up}$ and $H_c^{down}$ should be due to the trapped flux in the grains which generate a return field through the grain boundaries generating a lower effective field on the return branch and therefore a shift in the zero net field position. Hence, it should depend on the transport current since it depends on the trapped flux.

In figure 4, we also observe that, at low currents, the transition from the resistive state to zero resistance at approximately. $H_c^{down}$ is fairly sharp. It is seen from the evolution of the hysteresis loops that there is an asymmetry in $V_{\perp}$–$H$ curves with respect to zero field. The critical-field values $H_c^{up}$ which corresponds to $V_{\perp}$–$H$ curves measured for reversed direction are generally less than those of the ones measured for forward direction and are more closer to zero field value. At this point, we would like to note that, in the evolution of the $V$–$H$ curves, as the field is first swept in reverse and then in forward direction, this time it was observed that the asymmetry in

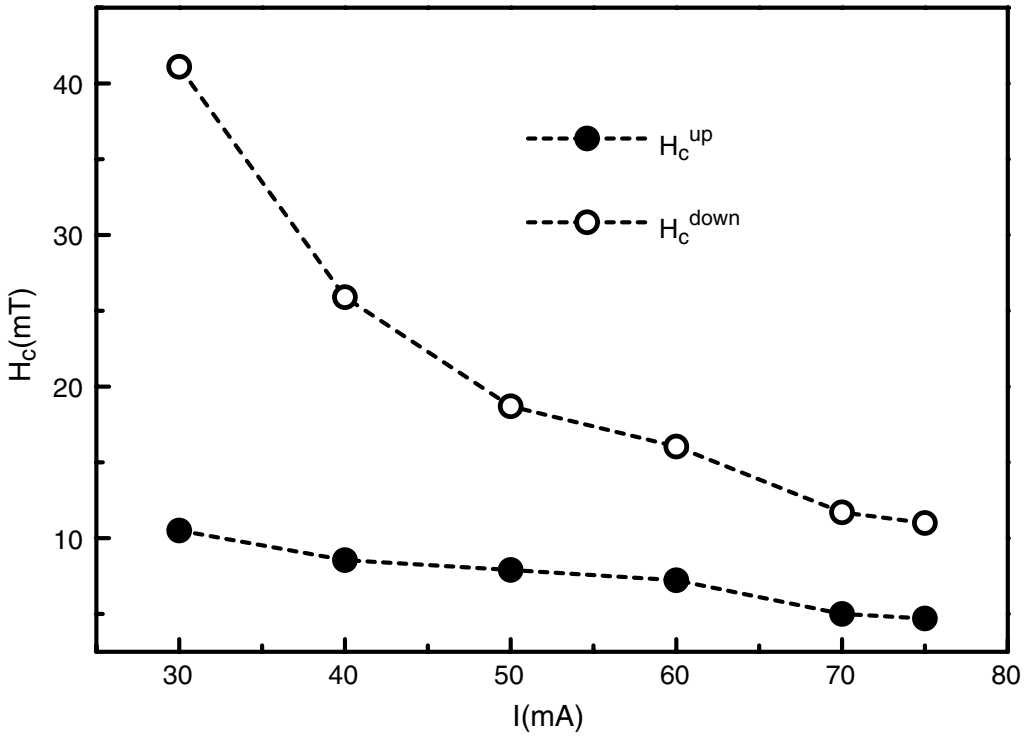


**Figure 5.** Current dependence of critical-field values $H_c^{up}$ and $H_c^{down}$ extracted from the curves in figure 4, which correspond to an increase in and decrease in sweeping of the magnetic field in the forward direction, respectively.

$V$–$H$ curves exchanges and $H_c^{up}$ values corresponding to the forward direction decrease. This means that the sample remains in a dissipative state for both directions when the applied magnetic field returns to zero. In addition, we suggest that the flux trapped inside the sample can give an extra voltage developing in the direction of the transport current.

## 4. Discussion

### *4.1. Hysteresis effects in V–H curves*

We first focus on the rapid increase in sample voltage developing in $V$–$H$ curves at low fields swept in both forward and reverse directions. It is seen from the $V$–$H$ curves that the nonlinearity which is a measure of dissipation rate correlated to $\sim \mathrm{d}V/\mathrm{d}H$ depends, mainly, on the temperature range, the magnitude of the transport current, field-sweep rate $\mathrm{d}H/\mathrm{d}t$, and also the field orientation with respect to the transport current. Starting from $H = 0$ and examining the initial branches of the hysteresis loops, we observe that the $V$–$H$ curves, except the ones for $V_{\|}$, generally tends to saturate for the field values above 10 mT. As the field is decreased, the $V$–$H$ curves become less resistive exhibiting strong irreversibilities.

The nonlinearity and the hysteresis effects which develop depending on several parameters given above will be discussed within the granular structure composing the sample. However, we note that the grains and their interfaces are not well-defined quantities and can differ from

crystallite to crystallite. In addition, the chemical and anisotropic states of the sample influence the transport and magnetic properties. It is widely assumed that a weak-link structure behaves like a type-II superconductor with its own penetration depth, its own first $H_{c1}{}^{W}$ and second critical field ($H_{c2}{}^{W}$), and also its own edge (surface-like) screening current flowing along the edge of the junction [5, 17, 37, 59, 74, 75], [83]–[86]. The junction parameters can be obtained from the low-field magnetization measurements ($M$–$H$) [17, 74, 75, 86]. The low-field $M$–$H$ measurements reveal that the critical field $H_{c1}{}^{W}$ has an order of a few 0.1 mT, whereas $H_{c2}{}^{W}$ has an order of a few 1 mT at low temperatures (i.e., 4.2 K) [17, 48]. These values are temperature-dependent and decrease with an increase in the temperature. Therefore, they are relatively small at the temperatures near $T_c$. In $V$–$H$ measurements, the field is ranging from 0 to 70 mT, and the minimum field-sweep rate is 1 mT $s^{-1}$. It must be expected for this sweep rate that the flux lines will penetrate into the sample very rapidly by disrupting completely the weak-link network. Along this dynamic process, the flux lines in the intergranular region where the weak-pinning regime exists will redistribute spatially themselves within a very short time leading to a correlated flux motion. As the field is increased further, the flux lines will gradually begin to penetrate into the grains from their weakest points. During the penetration, there will be a considerable competition between the pinning and depinning and the process will develop in favour of the pinning, since the grains have superconducting properties better than that of weak-link structure [5, 17, 36]. In this case, a slow variation of $V$ with $H$ is observed. Finally, in $V$–$H$ curves, it reaches a nearly steady state. In this regime, for different values of the transport currents, different constant flow rates associated with the flux entry and exit along the sample are nearly maintained.

In $V$–$H$ cycles, when the sample voltage saturates, the flux dynamics reach an equilibrium state in which there is no further increase in the average velocity of flux lines with increasing field. Within this description, the flux lines enter the sample from outside and traverse it by maintaining a constant flow rate, which leads to a correlated motion. Such a case, of course, depends on the magnitude of the driving current and temperature point to be investigated. As the field is decreased, an immediate drop in voltage away from the saturation level observed can lead to hysteresis effects. Although the external magnetic field is decreased, if there is no change in the measured dissipation, the physical case evolving through sample favours the reversible regime at the saturation region of $V$–$H$ cycles. In this case, the magnetic states of the sample do not change with decreasing magnetic field. However, further decrease in field strength can bring irreversibilities and the field value corresponding to the onset of departure from the saturation level can be taken to fall around the irreversibility line.

As the magnetic field is decreased, the voltage which corresponds to the decreasing branch of the field is lower than that of the increasing branch. Many researchers have attributed the strong hysteresis effects appearing in magnetoresistance measurements to the flux trapping inside the sample. For instance, Qian *et al* [55] interpreted the high-field hysteresis effects observed in polycrystalline YBCO sample in terms of the difference between local fields of $B_{up}$ and $B_{down}$ associated with the increasing and decreasing branches, respectively. They argued that the difference between $B_{up}$ and $B_{down}$ is a measure of the net magnetization of the grains by taking into account the demagnetization factor of the grains. Within this description, the observation of the hysteresis effects becomes possible provided that the local-effective field is greater than the critical field of $H_{c1}$. A similar discussion is given in recent studies by Mune *et al* [58], and also by Mahel and Pivarc [28]. We also note that such a physical description can be drawn from the two-level critical state model proposed by Ji *et al* [22], which considers the exact analytical calculations of the local fields of $B_{up}$ and $B_{down}$ in a granular structure. In addition, the hysteresis

effects have been observed not only at high fields, but also at the field range comparable to critical fields of weak-link network. Such a typical study has been reported by Chen and Qian [53]. Their explanation of the hysteresis effects in magnetoresistance measurements was based on the trapped flux in the loops comprised by superconducting grains and weak links between them. They assumed that the effective local field trapped inside the sample changes depending on the cycling of the external magnetic field up and down.

The hysteresis appearing in the $V$–$H$ curves represented in this study arises from the flux trapping and seems to be closely related to the difference in the local fields between the increasing and decreasing branches as pointed out by Ji *et al* [22] and Qian *et al* [55]. As the magnetic field is increased with a certain sweep rate, the flux lines penetrate into the sample from surface to interior. In increasing magnetic fields larger than the first critical field of the grains ($H_{cg}$), i.e., $H > H_{cg}$, a gradual flux penetration from intergranular region to the grains can develop along the special percolative paths correlated to the weak-pinning regions. As the magnetic field is ramped down, a reverse magnetic field through the grain boundaries will evolve due to the trapping of flux lines in the grains. In the decreasing branch of the $V$–$H$ curves, a considerable decrease in the effective local field compared to that of the increasing branch can develop due to the return flux going through the grain boundaries and generated by the trapped field in the grains, which leads to the hysteresis effects in the magnetovoltage curves. This also explains the symmetry of the $V$–$H$ curves where the field is cycled in forward and reverse directions, i.e., between $+H$ and $-H$ (see figure 4).

We would like to emphasize here that there is a flux motion not only along intergranular region, but also relatively along the weak-pinning centres inside the grains. As the magnitude of characteristic fields of the weak-link structure mentioned above is considered, an immediate destruction of the weak-link structure must be expected. We note that the flux lines do not enter the sample uniformly from the outer surface of the sample towards the interior, but will follow different stages starting from the surface barriers and the weakest paths of the weak-link network, and, finally, ending in the individual and highly superconducting grains. Then, there must be a partial penetration of flux lines into the grains along the weak-pinning regions, i.e., easy motion flow channels. The flux fronts will move towards the centre of grains and each individual grain behaves similar to a small single crystalline in this field range. We note that the sample edge in a single-crystalline sample corresponds to the grain boundaries in a polycrystalline sample. In our study, we use a polycrystalline YBCO sample and we suggest that these studies in addition to the experimental studies on single-crystalline samples and molecular dynamic simulations are also necessary for completeness and better understanding of the flux dynamics. Further, these studies serve as a benchmark for more complex systems, such as polycrystalline HTSCs samples. Due to the strong-pinning regime inside the grains, the flux motion evolving in these regions may be plastic rather than a correlated motion so that some of the flux lines are moving and the others remain pinned, and, further, depending on the pinning strength, development of a channel-like flow patterns spatially in different size can be expected. Many recent realistic computer simulations [87]–[92] and experimental studies support the formation of such easy motion channels for the flux lines [26], [72]–[75]. These studies show that the form of patterns depends mainly on the type and size of the pinning centres, pin density, temperature and the magnitude of the external driving force etc. When the effective size of the pinning centres are small, the flux lines can pass through the pinned flux lines without being trapped, that is, continue to flow between them, whereas the deflected vortices can be pinned if the pinning sites are too large. As the magnetic field is decreased, the number of the flux lines participating in the motion

and the size of the easy motion channels can decrease. This situation also implies that the pinning will become more effective.

We note that the stepwise structure and plateaux appearing in both the increasing and decreasing branches of the hysteresis loops (see figures 2, 3 and 4) give a further support for the formation of the channel-like patterns, and the presence of the plastic flow. In the plateau regions, although the external field increases, the effective velocity of the flux lines remains nearly constant for a while, which implies a constant flow rate. However, a further increase in magnetic field makes locally the correlated flux motion unstable and causes some of the flux lines to depin and, thus, an increase in the number of the mobile flux lines, which leads to the evolution of a stepwise structure. Reichhardt *et al* [88] have shown by using detailed molecular dynamic simulations that the vortex lattice interacting with periodic pinning array can lock to the various metastable states and give rise to such plateaux. Recent computer simulations performed [88, 93] and the experimental studies [59, 62] show the presence of similar plateaux and step structures in $I$–$V$ curves.

It is generally observed that the width of the plateaus in the increasing branch of the hysteresis loop are relatively greater than that of the decreasing one. The long-lived plateau regions evolve in the increasing branch, whereas, the relatively short-lived ones are observed for the decreasing branch. We suggest that the decrease in the external field and also the pinning cause a reduction in the number of mobile flux lines, and, thus, as a response against to the decrease in flux lines, the dynamic process cannot lock to a state for a long time, and the moving entity can be forced to change its state within a relatively short time together with the large irreversibilites.

### *4.2. Field-ramping rate ($\mathrm{d}H/\mathrm{d}t$) dependence of $V$–$H$ curves and correlations to time effects*

We now return to figures 1 and 2 to discuss the influence of the sweep rate on evolution of the hysteresis loops in detail. It can be suggested that the measurement of the $V$–$H$ curve should depend on the timescale of the experiment, in particular, on the time spent to plot the whole cycle. Therefore, it can be expected that the change in the sweep rate of the external field should reflect itself in $V$–$H$ curves as time effects (or relaxation effects). Due to the temperature and also field ranges investigated, the $V$–$H$ curves illustrated in figures 1 and 2 exhibit a field-sweep rate dependence. Figures 1(a)–(d) reveal that the decrease in $\mathrm{d}H/\mathrm{d}t$ from 13 to 1 mT s$^{-1}$ causes a remarkable increase in the area of the hysteresis loops of the $V_{\parallel}$ and $V_{\perp}$ curves. We suggest that, at high-sweep rates, the flux lines can have less time to find new accessible states, and, preferentially, the flux lines can follow nearly the same flow paths during the sweeping of the external magnetic field up and down, which leads to the observation of the reversible effects as in figure 1(a). On the other hand, with the field scale considered, we note that any remarkable change in dissipation depending on the sweep rates within the temperature and current ranges of the experiment is not observed for all $V$–$H$ curves represented in figures 1(a)–(d).

In a polycrystalline sample, it can be assumed that an energy landscape associated with the frustrated superconducting domains coupled by weak links includes a broad distribution of pinning barriers seen by mobile and immobile flux lines. Due to the driving force together with thermal activation, the flux lines in an inhomogeneous distribution of the energy landscape can easily overcome the neighbouring barriers by giving rise to a contribution to the measured dissipation but they may also fall in a deeper barrier and thus give no contribution to the measured voltage. However, at low-sweep rates, the flux lines find enough time for penetration and thus

an increase in the number of flux lines joining the motion causes an enhancement in measured dissipation. We notice that the relative strength of the random-pinning potential can be controlled by applying a driving current or by changing the magnetic field, and, the other parameter which influences the pinning potential is the temperature point to be investigated. One of the major roles of driving current is to lower the pinning barriers by creating nucleation centres for vortices. In figure 1, maximum driving current is 30 mA, while in figure 2, it is selected as 70 mA. We suggest that the driving current in figure 2 lowers pinning potential much more as compared to that of the one taken in figure 1, although the temperature in measuring the $V$–$H$ curves in figure 1 is higher than the temperature considered in figure 2. Thus, elastic and plastic deformations of the flux-line system at low-driving currents and sweep rates allow it energetically into deeper pinning potentials and thus the measured dissipation corresponding to lower sweep rates would decrease relatively.

A pronounced field-sweep rate dependence of $V_{\perp}$–$H$ curves is also represented in figure 2 where $\mathrm{d}H/\mathrm{d}t$ is varied from 1 to 5 mT s$^{-1}$. In contrast to the case seen in figures 1(a)–(d), at $T = 82.7$ K, it is observed that the $V$–$H$ curve measured at $\mathrm{d}H/\mathrm{d}t = 1$ mT s$^{-1}$ is more dissipative than that at 5 mT s$^{-1}$. For instance, as $\mathrm{d}H/\mathrm{d}t$ is varied from 5 to 1 mT s$^{-1}$, the relative increase in dissipation for the $V$–$H$ curve measured for the current value of $I = 70$ mA at $H = 50$ mT is $\sim$6%, whereas it is $\sim$1.5% for $I = 50$ mA at the same field value. It should be noted that the increase in dissipation at low-sweep rates appears at high values of the transport currents. As the transport current is decreased, the $V$–$H$ curves begins nearly to be independent of the sweep rate. It is possible to say that, therefore, the sweep-rate dependence of the dissipation in $V$–$H$ curves could not be observed in figure 1. The relative increase in dissipation observed at low-sweep rate in figure 2 can be explained as follows: if the field rate decreases, there is less relaxation, more effective trapped field in the grains, and thus more return flux and less effective field at the grain boundaries which, therefore, generates a situation with lower dissipation voltage.

It was shown experimentally that the low-field $M$–$H$ cycles are approximately independent of the sweeping rate of the magnetic field within the experimental accuracy and show no evidence of the relaxation of the Josephson vortices developing in the intergranular region [17] and, further, the time-dependent effects concerning the intergranular currents of granular materials are not observed at low-field $M$–$H$ measurements. As a first approximation, it can be suggested that the low-field $M$–$H$ and magnetovoltage curves are controlled by the same physical mechanisms. However, the time effects which may be related to the flux trapping in the grains could be observed in high-field $M$–$H$ measurements provided that $H$ has exceeded the true first critical field $H_{c1}$ [17]. Senoussi [17] showed that the size of the high-field $M$–$H$ loops expands dramatically at high-sweep rates of the external magnetic field, which implies a relative increase in the current carrying capacity of the sample. All these observations underline that, in order to see the effect of $\mathrm{d}H/\mathrm{d}t$ on the evolution of the $V$–$H$ curves, well-defined field-sweep rates, field and temperatures ranges are needed.

On the other hand, for these field and temperature ranges considered in this study, a negligible contribution of the field-sweep rate on the evolution of the shape of the $V_{\perp}$–$H$ curves is observed. To describe this physical situation, we consider again the channel-like flow patterns for flux lines which traverse the sample from one edge to another. As the current is set to a new higher value, the size of the channels begins to expand due to the Lorentz force and the number of the flux lines joining the flux motion effectively increase, since the net voltage measured is given by $V \sim N_{\mathrm{v}}\langle\nu\rangle$, where $N_{\mathrm{v}}$ is the number of the moving flux lines and $\langle\nu\rangle$ is their average velocity [62]. Thus, it can be expected that the flux lines follow nearly the same flow paths, but in

different size. This is the reason why a dramatic change is not observed in $V$–$H$ curves, although the transport current is varied.

### 4.3. Evolution of $V_{\parallel}$ curves

We also note that the evolution of the $V_{\parallel}$ and $V_{\perp}$ curves in figure 1 are nearly similar. Now, we discuss the dissipation appearing in $V$–$H$ curves when the external magnetic field is parallel to the transport current, i.e., $\vec{H} \parallel \vec{I}$. It is expected that the dissipation must be effectively zero for $\vec{H} \parallel \vec{I}$ since the Lorentz force is zero. However, the $V_{\parallel}$ curves illustrated in figures 1(a) and (c) reveal that the Lorentz force may not be actually zero and the condition of $\vec{H} \parallel \vec{I}$ is violated in polycrystalline HTSC samples and we attribute this violation to the highly anisotropic and layered structure of YBCO, which lower considerably the anisotropy of the driving current. On the other hand, in polycrystalline HTSC samples, the defects and imperfections to layered structure in grains and anisotropic states of the sample can perturb considerably the directions of local currents contributing to macroscopic current with the local field and can enhance the meandering motion along the sample. Thus, the condition of $\vec{H} \parallel \vec{I}$ cannot be satisfied on the macroscopic average by giving rise to a finite angle between $H$ and $I$ [94, 95]. We note that, for the same reason, the orthogonality between them cannot be satisfied.

Another effect is the large thermal fluctuations which lead to a liquid-like phase of flux-line system in high-temperature superconductors. Firstly, large thermal fluctuations can smooth considerably the energy barriers by reinforcing the flux motion. Secondly, the flux lines (also associated local currents) can be distorted locally and the condition of $\vec{H} \parallel \vec{I}$ can be destroyed as in the case of defects, imperfections, weak links etc. These two possible mechanisms can be the origin of the dissipation observed for $\vec{H} \parallel \vec{I}$ [94, 95].

### 4.4. Effect of transport current on the evolution of $V$–$H$ curves

Finally, we discuss the influence of the magnitude of the transport current on the evolution of the $V_{\perp}$–$H$ curves. In order to better represent the influence of the current and avoid any possible misunderstanding which may arise from the usual plots of the $V_{\perp}$–$H$ curves, each of them given in figure 3 were normalized to its voltage value corresponding to $H = 60$ mT. The normalized $V_{\perp}$–$H$ curves measured for the current values $I = 70$ and 30 mA at 83 and 86 K for $\mathrm{d}H/\mathrm{d}t = 1\ \mathrm{mT\ s^{-1}}$ are illustrated in figures 6(a) and (b) respectively. First of all, it is seen that figure 6 represents some extra details and describes the influence of the current on $V_{\perp}$–$H$ curves better. The curves reveal that the relative area of the hysteresis loops decreases with increasing transport current, which leads to diminution of the hyteresis effects. In addition, the dissipation associated with the curves measured for $I = 30$ mA continues to grow up with increasing magnetic field and the dissipation rate at this current value is greater than that of the current value of 70 mA for $H \gtrsim 5$ mT at $T = 86$ K and $H \gtrsim 10$ mT at $T = 83$ K respectively.

We note that the transport current plays a crucial role in the motional organization of flux lines and assumes the role played by the temperature in usual sense considered in statistical mechanics. Such an analogy between driving current and thermal fluctuations was investigated theoretically and studied numerically by solving the Langevin equation by Koshelev and Vinokur [96, 97]. At sufficiently high currents, the height of pinning potential is lowered by leading to motional ordering which could be observed in transport data [76, 79], and also in direct imaging experiments [98, 99]. We suggest that the plastic flow or plastic to elastic flow is also observed

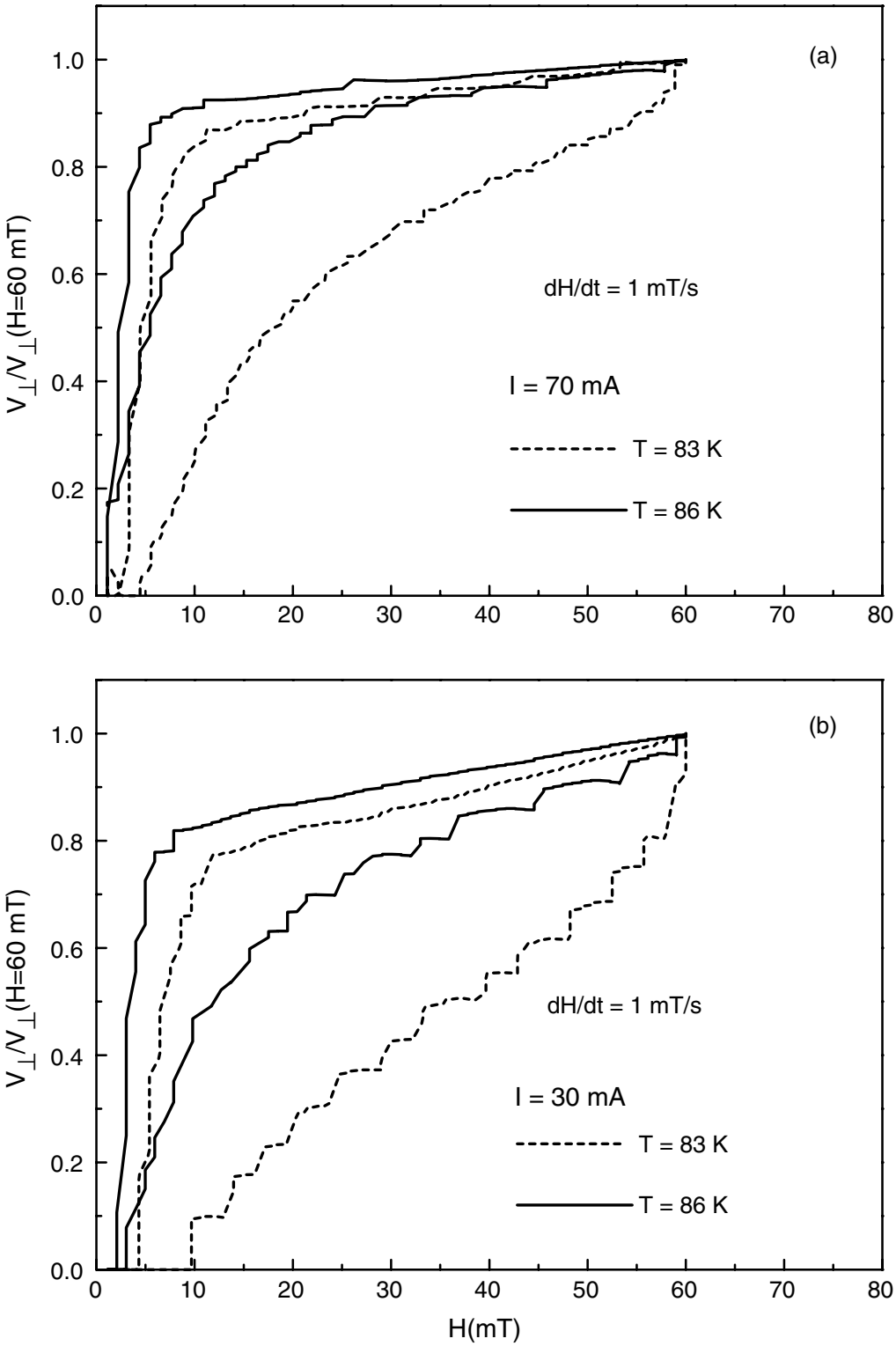


**Figure 6.** The normalization of $V_{\perp}$–$H$ curves given in figure 3 with respect to its corresponding voltage value at $H = 60\,\mathrm{mT}$. Note the decrease in the area of the hysteresis loop with increasing transport current. (a) $I = 70\,\mathrm{mA}$ at $T = 83$ and 86 K for $\mathrm{d}H/\mathrm{d}t = 1\,\mathrm{mT\,s^{-1}}$. (b) $I = 30\,\mathrm{mA}$ at $T = 83$ and 86 K for $\mathrm{d}H/\mathrm{d}t = 1\,\mathrm{mT\,s^{-1}}$.

in a stepwise structure together with the plateau regions of $V$–$H$ curves. The plateau regions correspond to locally correlated flux motion for a certain range of driving force; however, as the driving force is increased, some of the flux lines depin and the correlated motion becomes unstable. Thus, the flux lines are forced to move in another state which is stable in a range of driving force. After depinning of some of flux lines, firstly, a step structure evolves in the $V$–$H$ curves and then, another local correlated flux motion re-appears. On the other hand, the current dependence of the $V$–$H$ curves can be explained by the same argument of trapped field in the grains given above: if we increase the driving current, we effectively have less pinning since the pinning potential is reduced by the transport current and thus, it enables depinning of the flux lines by enhancing the correlated motion along the sample, therefore less trapped magnetic field and consequently less hysteresis.

A similar case is also seen for the $V_{\perp}$–$H$ curves measured at different temperatures. As can be seen from figure 6, for each current value, the width of the loops at $T = 86$ K is considerably less than that of the one at $T = 83$ K. On the other hand, we note that, from comparison of the curves in figures 3 and 6, the effect of temperature on the hysteresis loops measured at constant current is seen in both actual curves and normalized ones, although this behaviour, as is outlined above, is not apparent for the transport current. The higher temperature means higher thermal fluctuations and creep, and thus less trapped field and less hysteresis.

## 5. Conclusion

In this paper, below the critical temperature $T_c$, the hysteresis effects in magnetovoltage measurements ($V$–$H$ curves) in polycrystalline superconducting bulk sample of YBCO were investigated as a function of field orientation with respect to transport current, temperature, the magnitude of the transport current and the sweep rate of the external magnetic field ($\mathrm{d}H/\mathrm{d}t$). The strong clockwise hysteresis effects in the $V$–$H$ curves were interpreted within the granularity of sample mainly in terms of flux trapped in the grains returning through the grain boundaries. In well-defined field-sweep rates and temperature ranges a relative increase in measured dissipation could be observed at low values of $\mathrm{d}H/\mathrm{d}t$ depending on the current and it became possible to observe the relaxation effects in magnetovoltage measurements by varying the sweep rate of the external magnetic field, so that this underlines the importance of time spent to plot the whole cycle of the $V$–$H$ curves. This behaviour was attributed to fewer relaxation effects evolving in the grains and more effective trapped field in the grains, and, thus, more return flux and less effective field at the grain boundaries. On the other hand, the irreversible behaviour of the $V_{\perp}$–$H$ curves which manifests itself as an increase in the width of hysteresis loops increases at low currents and also at reduced temperatures. It was explained that high currents lower height of pinning barriers by causing less trapped field and, thus, less hysteretic effects. Similarly, the higher temperature increases thermal fluctuations and also flux creep by reducing the trapped field, and causes less hsyteresis in the $V$–$H$ curves.

## Acknowledgments

This work was supported by TUBITAK/TBAG 2037.

## References


[1] Peterson R L and Ekin J W 1988 *Phys. Rev.* B **37** 9848
[2] Evetts J E and Glowacki B A 1988 *Cryogenics* **28** 641
[3] Yeshurun Y and Malozemoff A P 1988 *Phys. Rev. Lett.* **60** 2202
[4] Dersch H and Blatter G 1988 *Phys. Rev.* B **39** 11391
[5] Tinkham M and Lobb J C 1989 *Solid State Phys.* **42** 91
[6] Mannhart J, Gross R, Hipler K, Huebener R P, Tsuei C C, Dimos D and Chaudhari P 1989 *Science* **245** 839
[7] Kes P H, Aarto J, van der Berg J, van der Beek C J and Mydosh J A 1989 *Supercond. Sci. Technol.* **1** 242
[8] Fisher M P A 1989 *Phys. Rev. Lett.* **62** 1415
[9] Koch R H, Foglietti V, Gallagher W J, Koren G, Gupta A and Fisher M P A 1989 *Phys. Rev. Lett.* **63** 1511
[10] Ji L, Rzchowski M S and Tinkham M 1990 *Phys. Rev.* B **42** 4838
[11] Dimos D, Chaudhari P and Mannhart J 1990 *Phys. Rev.* B **41** 4038
[12] Senoussi S, Hadjoudj S, Weyl C and Fondere J P 1990 *Physica* C **165** 199
[13] Zeldov E, Amer N M, Koren G, Gupta A, Mc Elfresh M W and Gambino R J 1990 *Phys. Rev. Lett.* **56** 680
[14] Kwok W K, Welp U, Crabtree G W, Vandervoort K G, Hulscher R and Liu J Z 1990 *Phys. Rev. Lett.* **64** 966
[15] Iye Y, Watanabe A, Nakamura S, Tamegai T, Terashima T, Yamamoto K and Bando Y 1990 *Physica* C **167** 278
[16] Askew T R, Flippen R B, Leary K J and Kunchur M N 1991 *J. Mater. Res.* **6** 1135
[17] Senoussi S 1992 *J. Phys. (Paris) III* **2** 1041
[18] Ricketts B W, Müller K H and Driver R 1991 *Physica* C **183** 17
[19] Kim D H, Miller D J, Holoboff R A, Kang J H and Talvacchio J 1991 *Phys. Rev.* B **44** 7607
[20] Gurevich A and Küpfer H 1993 *Phys. Rev.* B **48** 6477
[21] Thompson J R, Ren Sun Y, Civale L, Malozemoff A P, McElfresh M W, Marwich A D and Holtzberg F 1993 *Phys. Rev.* B **47** 14440
[22] Ji L, Rzchowski M S, Anand N and Tinkham M 1993 *Phys. Rev.* B **47** 470
[23] Mune P, Altshuler E, Musa J, Garcia S and Riera R 1994 *Physica* C **226** 12
[24] Li S, Fistul M, Deak J, Metcalf P and McElfresh M 1995 *Phys. Rev.* B **52** R747
[25] Fendrich J A, Welp U, Kwok W K, Koshelev A E, Craptree G W and Veal B W 1996 *Phys. Rev. Lett.* **77** 2073
[26] D'Anna G, Gammel P L, Safar H, Alers G B and Bishop D J 1995 *Phys. Rev. Lett.* **75** 3521
[27] Han G C and Ong C K 1997 *Phys. Rev.* B **56** 11299
[28] Mahel M and Pivarc J 1998 *Physica* C **308** 147
[29] Morozov N, Maley M P, Bulaevskii L N and Sarrao J 1998 *Phys. Rev.* B **57** R8146
[30] Göb W, Lang W and Sobolewski R 1998 *Phys. Rev.* B **57** R8150
[31] Landau I L and Ott H R 2000 *Physica* C **331** 1
[32] Paltiel Y, Zeldov E, Myasoedov Y N, Shtrikman H, Bhattacharya S, Higgins M J, Xiao Z L, Gammel P L and Bishop D J 2000 *Nature (London)* **403** 398
[33] Haslinger R and Joynt R 2000 *Phys. Rev.* B **61** 4206
[34] Sukhanov A A and Omelchenko V I 2001 *Low Temp. Phys.* **27** 609
[35] Bobyl A V, Shantsev D V, Galperin Y M, Johansen T H, Baziljevich M and Karmanenko S F 2002 *Supercond. Sci. Technol.* **15** 82
[36] Hilgenkamp H and Mannhart J 2002 *Rev. Mod. Phys.* **74** 485
[37] Clem J R 1988 *Physica* C **153–155** 50
[38] Gurevich A, Rzchowski M S, Daniels G, Patnaik S, Hinaus B M, Carillo F, Tafuri F and Larbalastier D C 2002 *Phys. Rev. Lett.* **88** 097001
[39] Malozemoff A P, Manhart J and Scalapino D 2005 *Phys. Today* (April) 41
[40] Larbalastier D, Gurevich A, Felgmann D M and Polyanskii A 2001 *Nature* **414** 368
[41] Norton D P *et al* 1996 *Science* **274** 755
[42] Palau A *et al* 2004 *Appl. Phys.* **84** 230

[43] Feldmann D M *et al* 2000 *Appl. Phys. Lett.* **77** 2906
[44] Feldmann D M *et al* 2001 *Appl. Phys. Lett.* **79** 3998
[45] Verebelyi D T, Christen D K, Feenstra R, Cantoni C, Goyal A, Lee D F, Arendt P N, Paula D F, Groves J R and Prouteau C 2000 *Appl. Phys. Lett.* **76** 1755
[46] Senoussi S, Oussena M and Hadjoudj S 1988 *J. Appl. Phys.* **63** 4176
[47] Senoussi S, Aguillon C and Manuel P 1991 *Physica* C **175** 202
[48] Senoussi S, Aguillon C and Hadjoudj S 1991 *Physica* C **175** 215
[49] Senoussi S, Kilic A, Manuel P, Gagnon R, Taillefer L and Traxler H 1996 *Physica* C **264** 172
[50] Prozorov R, Poddar A, Sheriff E, Shaulov A and Yeshurun Y 1996 *Phsyica* C **264** 27
[51] Sheriff E, Prozorov R, Yeshurun Y, Shaulov A, Koren G and Chabaud-Villard C 1997 *J. Appl. Phys.* **82** 4417
[52] McHencry M E, Maley M P and Willis J O 1989 *Phys. Rev.* B **40** 2666
[53] Chen K Y and Qian Y J 1989 *Physica* C **159** 131
[54] Xia J S, Sun S F, Zhang T, Cao L Z, Zhang Q R, Chen J and Chen Z Y 1989 *Physica* C **158** 477
[55] Qian Y J, Zhang Z M, Chen K Y, Zhou B, Qui J W, Miao B C and Cai Y M 1989 *Phys. Rev.* B **39** 4701
[56] Kwasnitza K and Widmer Ch 1990 *Physica* C **171** 211
[57] Cai X Y, Gurevich A, Tsu I-F, Kaiser D L, Babcock S E and Larbalastier D C 1998 *Phys. Rev.* B **57** 10951
[58] Mune P, Foncesa F C, Muccillo R and Jardim R F 2003 *Physica* C **390** 363
[59] Kiliç A, Kiliç K and Çetin O 2003 *Physica* C **384** 321
[60] Habbal F and Joiner W C H 1978 *J. Low. Temp. Phys.* **32** 239
[61] Campbell A M and Evetts J E 1971 *Adv. Phys.* **21** 200
[62] Bhattacharya S and Higgins M J 1995 *Phys. Rev.* B **52** 64
[63] Hellerqvist M C, Ephron D, White W R, Beasley M R and Kapitulnik A 1996 *Phys. Rev. Lett.* **76** 4022
[64] Beloborodov I S, Efetov K B and Larkin A I 2000 *Phys. Rev.* B **61** 9145
[65] Gerber A, Milner A, Deustscher G, Karpovsky M and Gladkikh A 1997 *Phys. Rev. Lett.* **78** 4277
[66] Han G C and Ong C K 1997 *Phys. Rev.* B **56** 11299
[67] Safar H, Gammel P L, Huse D A, Majumdar S N, Schneemeyer L F, Bishop D J, Lopez D, Nieva G and de la Cruz F 1994 *Phys. Rev. Lett.* **72** 1272
[68] Lopez D, Nieva G and de la Cruz F 1994 *Phys. Rev.* B **50** 7219
[69] Righi E F, Grigera S A, Lopez D, Nieva G, De la Cruz F, Civale L, Pasquini G and Levy P 1997 *Phys. Rev.* B **55** 5663
[70] Grigera S A, Morre E, Osquiguil E, Nivea G and de la Cruz F 1999 *Phys. Rev.* B **59** 11201
[71] Grigera S A, Grigera T S, Righi E F, Nieva G and de la Cruz F 2002 *Physica* C **371** 237
[72] Danckwerts M, Gon A R and Thomsen C 1999 *Phys. Rev.* B **59** R6624
[73] Xiao Z L, Andrei E Y, Shuk P and Greenblatt M 2001 *Phys. Rev. Lett.* **86** 2431
[74] Kiliç K, Kiliç A, Yetiç H and Çetin O 2003 *Phys. Rev.* B **68** 144513
Kiliç K, Kiliç A, Yetiç H and Çetin O 2003 *Virtual J. Appl. Supercond.* **5** (8)
[75] Kiliç K, Kiliç A, Yetiç H and Çetin O 2004 *J. Appl. Phys.* **95** 1924
[76] Henderson W, Andrei E Y, Higgins M J and Bhattacharya S 1996 *Phys. Rev. Lett.* **77** 2077
[77] Kiliç A, Kiliç K and Çetin O 2003 *J. Appl. Phys.* **93** 448
Kiliç A, Kiliç K and Çetin O 2003 *Virtual J. Appl. Supercond.* **4** (1)
[78] Karimov Yu S and Kikin A D 1990 *Physica* C **169** 50
[79] Xiao Z L, Andrei E Y and Higgins M J 1999 *Phys. Rev. Lett.* **83** 1664
[80] Zhang Y H, Luo H, Wu X F and Ding S Y 2001 *Supercond. Sci. Technol.* **14** 346
[81] Feigel'man M V, Geshkeinbein V M, Larkin A I and Vinokur V M 1989 *Phys. Rev. Lett.* **63** 2303
[82] Ma L P, Li H C and Li L 1997 *Physica* C **291** 143
[83] Ferrel R A and Prange R E 1963 *Phys. Rev. Lett.* **10** 479
[84] Josephson B D 1964 *Rev. Mod. Phys.* **36** 216
[85] Clem J R, Bumble B, Raider S I, Gallagher W J and Shih Y C 1987 *Phys. Rev.* B **35** 6637
[86] Kiliç A, Kiliç K and Senoussi S 1998 *J. Appl. Phys.* **84** 3255

[87] Koshelev A E 1992 *Physica* C **198** 371
[88] Reichhardt C, Olson C J, Groth J, Field S and Nori F 1996 *Phys. Rev.* B **52** R8898
[89] Olson C J, Reichhardt C, Groth J, Field S B and Nori F 1997 *Physica* C **290** 89
[90] Olson C J, Reichhardt C and Nori F 1997 *Phys. Rev.* B **56** 6175
[91] Reichhardt C, Olson C J and Nori F 1997 *Phys. Rev. Lett.* **78** 2648
[92] Olson C J, Reichhardt C and Nori F 1998 *Phys. Rev. Lett.* **80** 2197
[93] Cao Y, Jiao Z and Ying H 2000 *Phys. Rev.* B **62** 4163
[94] Brandt E H 1995 *Rep. Prog. Phys.* **58** 1465
[95] Kiliç A, Kiliç K, Senoussi S and Demir K 1998 *Physica* C **294** 203
[96] Koshelev A E and Vinokur V M 1994 *Phys. Rev. Lett.* **73** 3580
[97] Xiao Z L, Andrei E Y, Shuk P and Greenblatt M 2000 *Phys. Rev. Lett.* **85** 3265
[98] Koblischka M R, Schuster Th and Kronmüller H 1994 *Physica* C **219** 205
[99] Jooss Ch, Albrecht J, Kuhn H, Leonhardt S and Kronmüller H 2002 *Rep. Prog. Phys.* **65** 651